NANO LETTERS

pubs.acs.org/NanoLett Letter

Self-Powered High-Responsivity Photodetectors Enhanced by the Pyro-Phototronic Effect Based on a $BaTiO_3$/GaN Heterojunction

Yueming Zhang, Jie Chen, Laipan Zhu,* and Zhong Lin Wang*

Cite This: https://doi.org/10.1021/acs.nanolett.1c03171 Read Online

ACCESS | Metrics & More | Article Recommendations | Supporting Information

ABSTRACT: Perovskite and semiconductor materials are always the focus of research because of their excellent properties, including pyroelectric, photovoltaic effects, and high light absorption. On basis of this, the design of combining $BaTiO_3$ (BTO) thin films with a GaN layer to form a heterojunction structure with a pyro-phototronic effect has achieved an efficient self-powered BTO/GaN ultraviolet photodetector (PD) with high responsivity and a fast response speed. With cooling and prepolarization treatments, the photocurrent peak and plateau have been enhanced by up to 1348 and 1052%, and the response time of the pyroelectric and common photoelectric current are improved from 0.35 to 0.16 s and from 3.27 to 2.35 s with a bias applied, respectively. The self-powered BTO/GaN PD combined with a pyro-phototronic effect provides a new idea and optimization for realizing ultrafast ultraviolet sensing at room temperature, making it a promising candidate in environmentally friendly and economical ultraviolet optoelectronic devices.

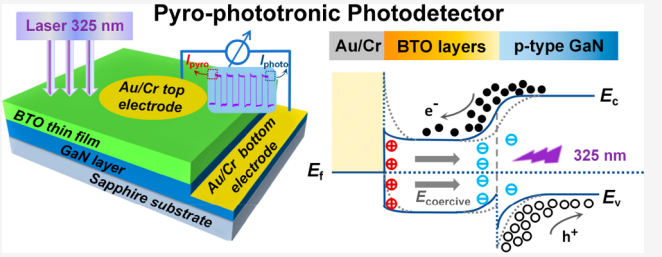

KEYWORDS: *BTO/GaN heterostructure, photodetector, ferroelectric, pyro-phototronic effect, ultraviolet sensing*

1. INTRODUCTION

As one of the most widely investigated perovskite materials, $BaTiO_3$ (BTO) has been commonly applied in various fields, including electrocaloric refrigeration,[1−3] energy storage,[4−7] dielectric tuning,[8,9] and various sensing.[10−14] Because of the multifarious physical characteristics owned by BTO, such as ferroelectric,[15,16] piezoelectric,[17,18] thermoelectric,[19,20] pyroelectric,[21,22] and photovoltaic properties,[23−25] there has been significant progress in the conversion from light, heat, and pressure to an electrical signal. Furthermore, it is this kind of mutual coupling of various characteristics that overcomes the disadvantages caused by only single-source conversion in the past. Thus, it is necessary to take advantage of this multimechanism coupling to optimize related applications. Among these applications, room-temperature photoelectric detection has sparked an increasing interest for developing low-power and self-powered nanodevices, which involves multiple energy conversions above.[26−28] Therefore, only relying on the multimechanism coupling method can better satisfy the growing demand for advanced optoelectronic applications.

Because the BTO always undergoes a transition from the cubic paraelectric phase to the tetragonal ferroelectric phase with a temperature variation, revealing a prominent spontaneous polarization along its *c*-axis, the pyroelectric potentials induced by temperature changes across the material can be keenly detected because of the noncentral structure symmetric crystal structures of *P4mm* BTO.[29,30] Specifically, when the sample is suddenly exposed to light illumination, there will be a sharp rise in temperature, which will cause a deformation of material due to thermal expansion and contraction, then leading to a distribution of pyroelectric potential along the crystal with polarized pyro-charges presenting at the upper and lower interfaces because of the reinforced asymmetry of BTO. In a sense, the pyro-phototronic effect is a form that can be traced back to the piezoelectric effect. However, there are quite a few applications of BTO in photoelectric detection reported compared to other typical properties. In recent years, some exciting progresses have been made in photoelectric detector;[10,11,31,32] however, the only fly in the ointment could be the low responsivity compared to classical PDs.[33,34] To further enhance the signal strength and sensitivity of the BTO-based PD, a new approach is thus introduced to enhance the charge−carrier transport process during the optoelectronic processes by improving the light absorption and utilizing the pyroelectric polarizations, which is always called the pyro-phototronic effect and was commonly found in ZnO piezoelectric systems in the past.[35−37] However, the selection of a BTO system will make the pyroelectric effect more

Received: August 16, 2021
Revised: October 2, 2021

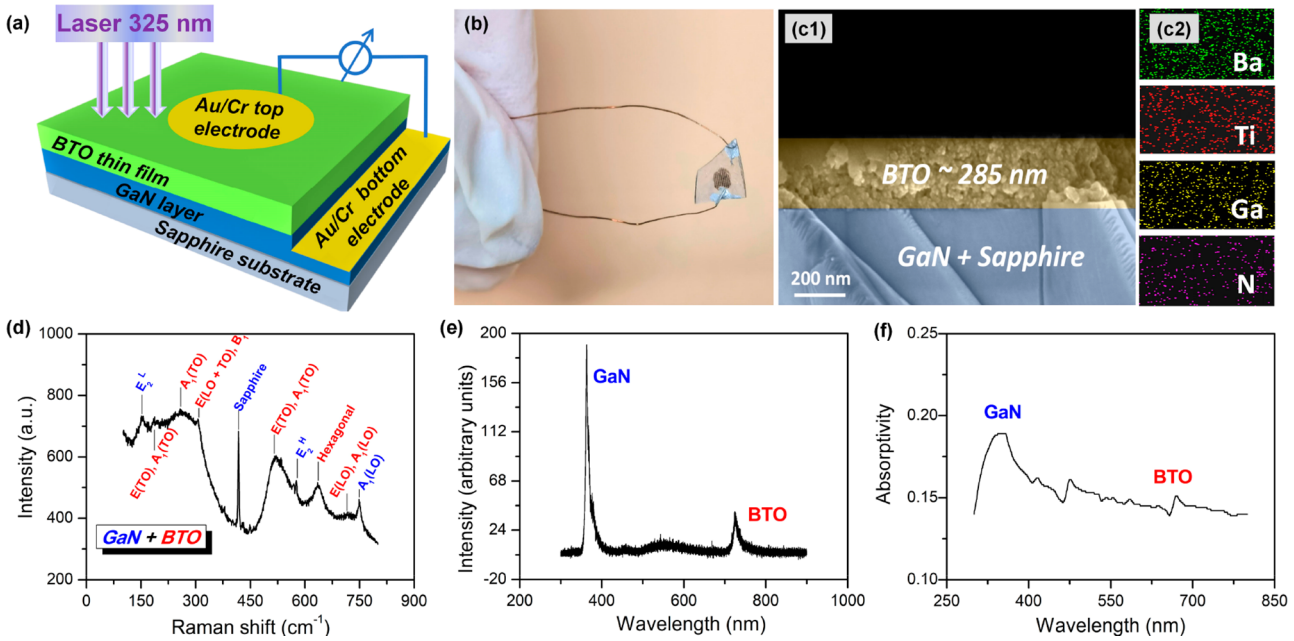

Figure 1. Structure and characterization of the BTO/GaN thin-film PD. (a) Schematic illustration of the structure of the self-powered BTO/GaN PD. (b) Photograph of the BTO/GaNPD. (c1) Thickness of the fabricated BTO/GaN PD observed by a cross-sectional SEM image. (c2) Energy-dispersive spectrometer of the BTO/GaN thin film. (d) Raman spectrum of the perovskite (BTO) on the GaN layer. (e) Photoluminescence spectrum of the BTO/GaN PD. (f) Absorption spectrum of the BTO/GaN PD under UV−vis irradiation.

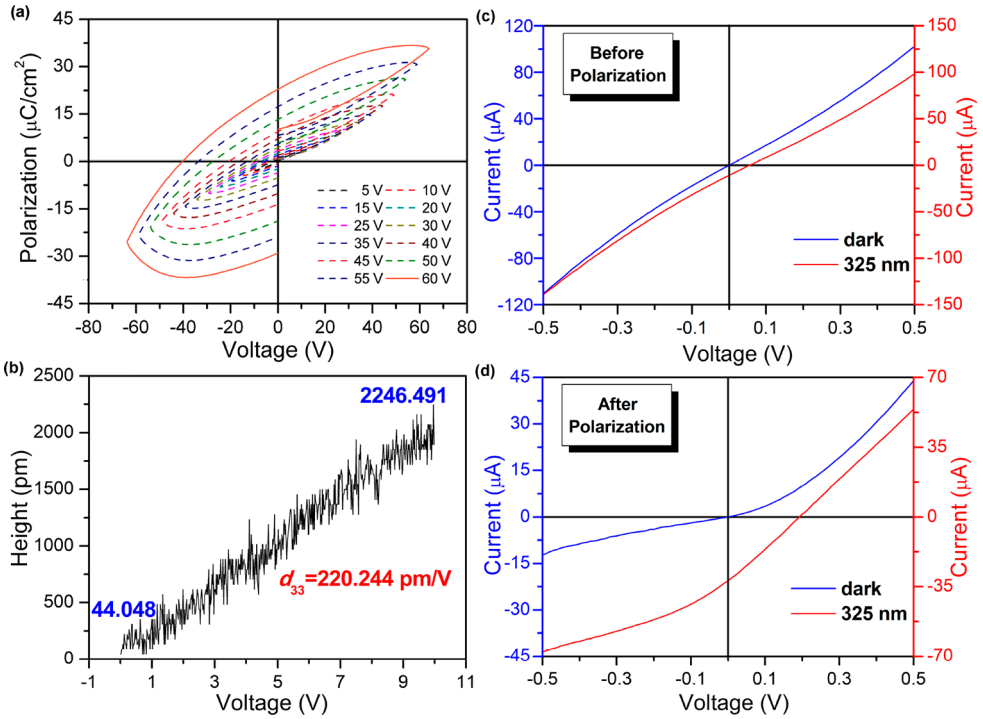

Figure 2. Basic electrical properties of the BTO/GaN thin film. (a) *P*−*E* loops of the BTO/GaN thin film at selected voltages. (b) Piezoelectric curve of the BTO/GaN thin film measured by an AFM. *I*−*V* characteristics of the self-powered BTO/GaN PDs under dark and 325 nm laser illumination with a power density of 4.68 mW/cm^2 (c) before polarization and (d) after polarization at 10 V for 10 min.

optimized because of the spontaneous polarization within the material.[38,39]

In this work, the light-self-induced pyroelectric and photoelectric effects are used to modulate the optoelectronic processes, thus enhancing the performances of ultraviolet sensing. We chose to combine the BTO thin films (approximately nanometer) rather than traditional BTO ceramic sheets (approximately micrometer to millimeter) with the third-generation semiconductor GaN, so that the system can be driven by a larger self-polarized electric field ($E = U/d$) inside the BTO thin films.[40] In addition to the intrinsic characteristics of GaN, including wide direct bandgap, high breakdown voltage, large absorption coefficient, and high carrier mobility, GaN is utilized to form a heterostructure with

https://doi.org/10.1021/acs.nanolett.1c03171
Nano Lett. XXXX, XXX, XXX−XXX

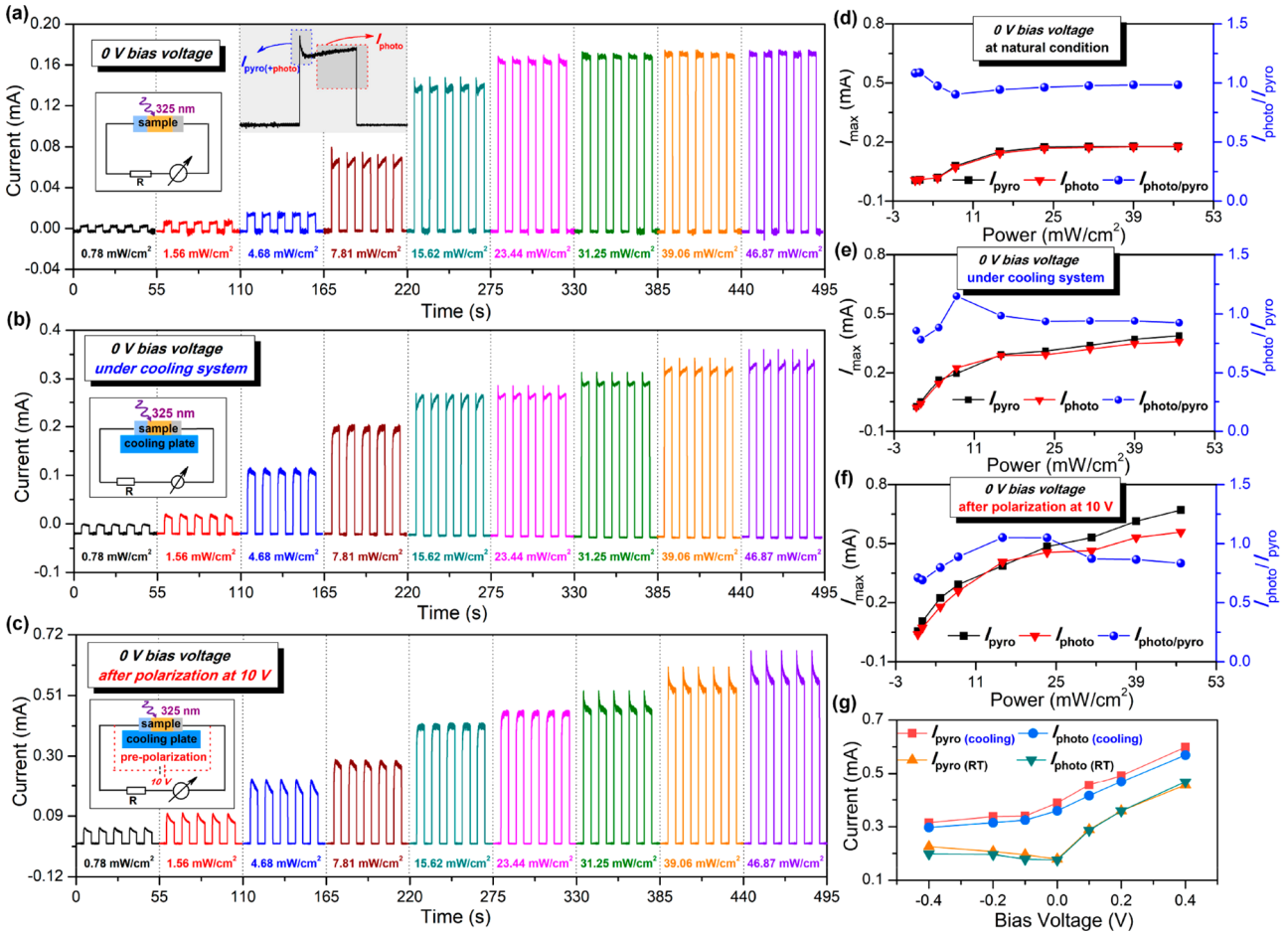

Figure 3. Performance of the self-powered BTO/GaN thin-film PDs. (a) $I-t$ characteristics of the self-powered BTO/GaN PDs under only 325 nm illuminations with different power densities from 0.78 to 46.87 mW/cm^2 at natural conditions; the insets are the schematic diagram of the test and the enlarged $I-t$ curves under 4.68 mW/cm^2. (b) $I-t$ characteristics of BTO/GaN PDs under a "light + cooling" system; the inset is the schematic diagram of the test. (c) $I-t$ characteristics of the BTO/GaN PDs under a "light + cooling" system after prepolarization at 10 V for 10 min; the inset is the schematic diagram of the test. (d–f) Numerical extraction of I_{pyro} and I_{photo} from a–c; the right side is the change in I_{photo}/I_{pyro} under corresponding condition. (g) Comparison of the $I-t$ characteristics at different bias voltages with the maximum illumination power density under natural conditions (no polarization and at room temperature (RT)) and under a cooling system (cooling), respectively.

BTO thin films as self-powered PDs.[41−45] With cooling and prepolarization treatments, the photocurrent peak and plateau have been enhanced by up to 1348 and 1052%, and the response times of the pyroelectric and the common photoelectric current are improved from 0.35 to 0.16 s and from 3.27 to 2.35 s with a bias applied, respectively. The self-powered BTO/GaN PD combined with the pyro-phototronic effect provides a new idea and optimization for realizing ultrafast ultraviolet-sensing at room temperature, making it a promising candidate in environmentally friendly and economical ultraviolet optoelectronic devices.

2. RESULTS AND DISCUSSIONS

2.1. Structure and Basic Electrical Properties. The design of the self-powered BTO/GaN thin-film PD is schematically demonstrated in Figure 1a, including a lower GaN grown on sapphire as a substrate, BTO thin films and electrode arrangements. Figure 1b shows a photograph of the test unit of BTO/GaN PD, which consists of the sample and wires leading from the upper and lower electrodes stuck with silver paste, making it convenient for the later electrical testing. Figure 1c1 and Figure S1a, b are the SEM images of the cross section and the surface at high magnification, illustrating the thickness of 285 nm and the general particle size diameter of 30−80 nm. The element mapping and amount of BTO thin films along with the corresponding energy-dispersive spectroscopy (EDS) diagrams are shown in Figure 1c2 and Figure S1c. The microstructure of BTO/GaN is verified by taking the Raman spectrum (Figure 1d) and XRD patterns (Figure S 1d); the characteristic peaks of BTO and GaN are superimposed and coexist rather than interfering with each other. According to the photoluminescence (PL) spectra in Figure 1e, it can be roughly estimated by the position of the obvious peaks that the band gaps of GaN and BTO ($P4mm$) are 3.4 and 1.8 eV,[46,47] respectively, which are exactly in line with the standard band gap of conventional GaN and BTO corresponding to the dominant $P4mm$ space group. In addition, it can be found that there exist some indistinct peaks at wavelengths of 470 and 520 nm in the Raman spectrum, which corresponds to the orthorhombic phase $Amm2$ and trigonal phase $R3m$ space group (band gap ∼2.3−3.2 eV), providing the material with spontaneous polarization.[48] Additionally, the position of the main characteristic peaks in the UV−vis spectrum (Figure 1f) are consistent with those obtained by the PL spectrum, and some of the heteropeaks are related to the structure of

https://doi.org/10.1021/acs.nanolett.1c03171
Nano Lett. XXXX, XXX, XXX−XXX

multiphase coexistence of BTO films because of the free growth during the sol−gel fabrication.

Figure 2a presents $P-E$ loops of the BTO/GaN thin films at selected electric fields, behaving as obvious ferroelectrics that possess both large residual polarizations (P_r) and strong coercive fields (E_C) along the direction from BTO to GaN, which provides the basis for generating the pyroelectric signal. However, it can be found that the $P-E$ loops of this sample are asymmetrical and wider compared with the typical ferroelectric hysteresis loop, indicating the leakage current of this sample is relatively large with an increasing applied electric field, which makes it possible to detect the light-induced current. The piezoelectric coefficient d_{33} of the BTO/GaN is shown as Figure 2b, where the measured and fitted value of d_{33} is 220.224 pm/V according to the inverse piezoelectric effect, which will provide strong support to the pyroelectric effect. $I-V$ characteristic curves of the sample under a 325 nm light illumination before and after polarization at 10 V for 10 min are plotted in Figures 2c and d. In comparison with the dark current (blue curve), the 325 nm illumination current (red curve) almost coincides with it, showing a slight ferroelectric photovoltaic effect before polarization.[49] However, with the prepolarization applied at 10 V for 10 min, both curves show obvious rectifying characteristics, and the Y-intercept of red curve increases, indicating a more conspicuous ferroelectric photovoltaic effect than that of the sample before polarization. In other words, prepolarization can be understood as a process of charging the device, thus providing a greater driving force for the self-actuated photoelectric response of the BTO/GaN thin-film PD.

2.2. General Performances of the Self-Powered BTO/GaN Thin-Film PDs. The systematic research and summary on current responses of the self-powered BTO/GaN thin-film PD to ultraviolet illumination at room temperature (RT) are plotted in Figure 3a, showing a continuous increase in both the current peaks and current plateaus with increasing illumination intensity from 0.78 to 46.87 mW/cm^2. As the upper inset illustrated in Figure 3a, the current response can be divided into two stages under each power intensity. The first stage consists of a sharp peak induced by pyroelectric (referred as I_{pyro}: the value of an instantaneous response at the rising edge is denoted as I_{pyro}) because of its faster response than ordinary photocurrent, and the second stage mainly consists of a steady current plateau (referred to as I_{photo}: the value when the current reaches stability is denoted as I_{photo}). The extractions of corresponding currents are plotted in Figure 3d as black and red dots to present changes in output signals with varying power intensity. It can be obviously found that both currents I_{pyro} and I_{photo} show a monotonous increasing trend as the power intensity of the illumination rises, and the I_{pyro} is larger than I_{photo} at all illumination statements. However, the contributions of I_{pyro} and I_{photo} to the overall output response vary in portion under different conditions. When the illumination stays at a low power density, at which it is hard to cause a remarkable instantaneous temperature rise within the sample, the I_{photo} as the main force of the signal output accounts for a large proportion. With the enhancement of the power density, an instantaneous increase in temperature within the sample will occur as the laser beam opened, leading to a fast responsive sharp peak of I_{pyro} to make it more important in the signal output process. As the power density continues to rise, the I_{pyro} and I_{photo} all gradually reach the saturation state, making almost the same contributions to the output signal, which means the sharp peaks of I_{pyro} will be blurred again. To further investigate the enhancement of the pyroelectric effect on the performances of BTO/GaN thin-film PDs, we applied different biases considering the coercive field derived from the spontaneous polarization. The stable and repeatable current responses to selected biases under different illumination conditions are shown in Figure S2a. Generally, the intensity of both pyroelectric and photoelectric signals increases with the laser power density elevated at all biases, which is similar to the response at zero bias under natural conditions. It can be seen in Figure S2b that the signal strength obtained under positive bias is stronger than that under negative bias, and the value of I_{photo}/I_{pyro} is smaller at the negative bias, which means that the pyroelectric effect is more obvious under this condition.

During the testing, different time intervals between each measuring period were adopted in the measurement under zero bias with a 7.81 mW/cm^2 illumination power density as shown in Figure S3a, every 5, 10, 15, and 20 s, respectively. It can be observed that the intensity of the pyroelectric signal decays greatly when the interval time is short; however, it can be returned to the original strength without obvious attenuation with the extension of interval time. The reason for this is that the heat is not released completely in a short period of time, resulting in heat accumulation, so that the temperature change caused by the next laser irradiation is small, leading to the reduction of the pyroelectric peak. To dissipate the heat as quickly as possible to get rid of the heat accumulation for further optimization, a cooling system was introduced to the testing process, which can not only enhance the pyroelectric potential difference at interfaces because of the cold contraction but also extend carrier life to ensure the stability of the enhanced current. The cooling system is shown as Figure S3b, which can cause a reduction from room temperature to about 10 °C ($\Delta T = -18$ K) shown as Figure S3c. On the basis of the testing condition as the inset in Figure 3b illustrated, the current peaks (I_{pyro}) and current plateaus (I_{photo}) signals can be respectively increased from 0.18 to 0.39 mA and from 0.17 to 0.36 mA after the PD was equipped with the cooling system. Meanwhile, the shape of the peak also changed; the cooling system will make the PD more sensitive to the illumination at low power density. The pyroelectric current peak can be clearly monitored from 0.78 to 4.68 mW/cm^2 and from 15.62 to 46.87 mW/cm^2 but is indistinct under 7.81 mW/cm^2, and there always exists a mutation in the I_{photo}/I_{pyro} diagram (shown as Figure 3e), indicating that there is a threshold value of power density for the responsivity of the PD to the pyroelectric effect and photoelectric effect. When the power density is between the threshold value, the growth ratio of I_{photo} is greater than that of I_{pyro} and the intensity photocurrent signal is greater than that of pyroelectric signal, so it is difficult to be observe the pyroelectric current peak. When the laser power density is outside this threshold, the results are opposite. The principle of the current response at all biases under the cooling system is similar to that at room temperature, and the responsivity increases to a greater extent with the bias enhanced as shown in Figure S4.

Because of the high responsivity and fast response rate of I_{pyro}, which is expected to be further enhanced, a prepolarization supplied by a 10 V DC power for 10 min along with the cooling system were applied (shown as the inset in Figure 3c) before testing to better strengthen the coercive field within the material. Both the current peak and the current plateau were

https://doi.org/10.1021/acs.nanolett.1c03171
Nano Lett. XXXX, XXX, XXX−XXX

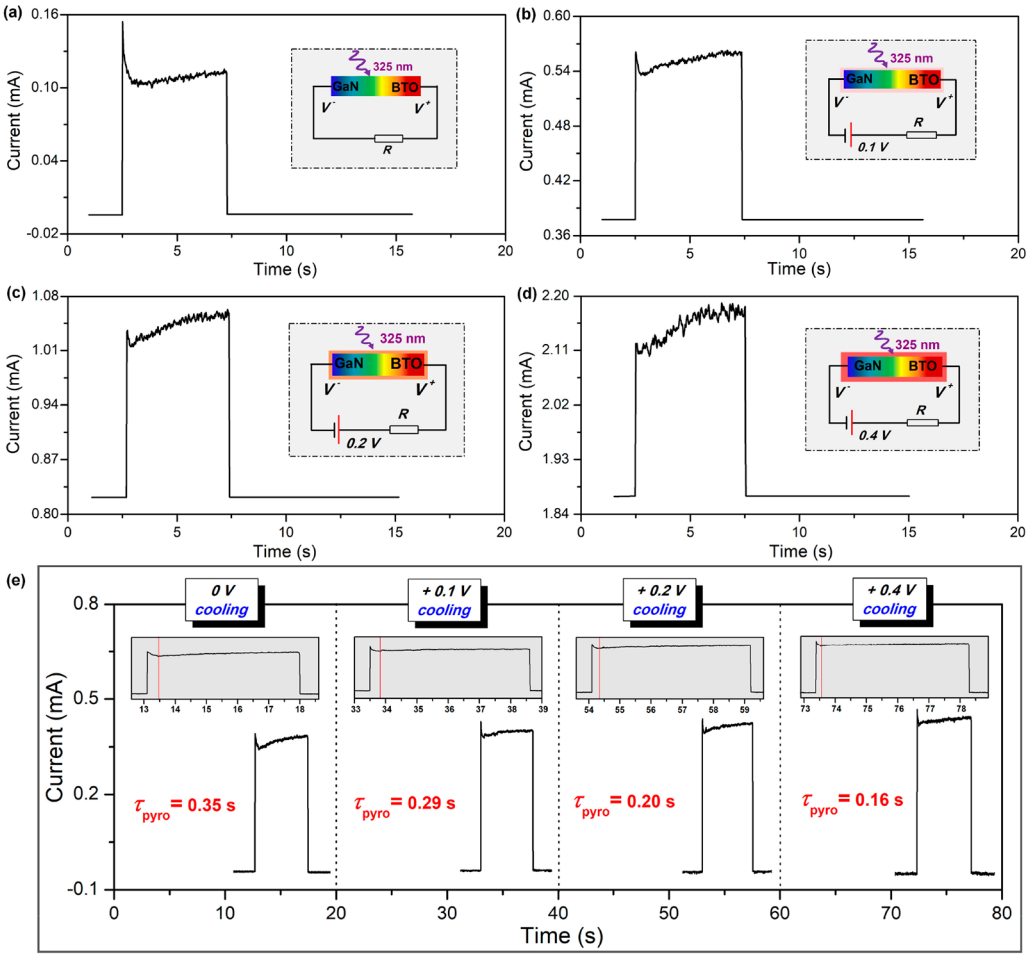

Figure 4. Pyro-phototronic performance of the self-powered BTO/GaN thin-film PDs at different biases. (a–d) I–t curves of the BTO/GaN PDs under 325 nm illuminations with 15.62 mW/cm^2 at different biases of (a) 0.0, (b) 0.1, (c) 0.2, and (d) 0.4 V to represent the influence of bias on I_{pyro} and I_{photo}. The insets indicate the corresponding circuit diagrams with current heating effect and pyro-phototronic effect of BTO (the glow around BTO/GaN). (e) Response time extraction of I_{pyro} and I_{photo} under both 325 nm illuminations with 31.25 mW/cm^2 and a cooling system at different biases. Insets: magnified x-axis views of the instantaneous response.

dramatically improved from 0.18 to 0.67 mA and from 0.17 to 0.56 mA, respectively (shown as Figure 3f), after prepolarization under the cooling system. Moreover, even at low temperature with low power density, both the pyroelectric current peak and the common photocurrent plateau can be detected more obviously than that under natural statements or just single cooling conditions. Similarly, there are upper and lower threshold boundaries for the laser power density during the test as illustrate above.

The comparison of the I–t characteristics at different bias voltages under natural conditions (no polarization and at room temperature (RT)) and under a cooling system (cooling) is shown in Figure 3g. It can be found that when a positive bias is applied (in the same direction as the electric field generated by spontaneous polarization within the material), the output signal strength will increase with the increasing applied bias under both conditions. Nevertheless, when an electric field is applied in the opposite direction to that generated by spontaneous polarization within the material, the resulting electric field inside the material can be canceled or even reversed. When the device is under a cooling system, the larger polarized electric field induced by the cold shrinkage with the material is not easily completely canceled by the reverse applied electric field, but the larger the applied reverse electric field is, the smaller the remaining electric field will be, so the output signal strength will weaken with the enhancement of the reverse field. However, when the device is under natural conditions, the polarization field inside the material is relatively small and can be easily canceled or even reversed. Therefore, when the applied reverse electric field exceeds the cancellation value, the signal will be enhanced again. The application of bias can not only enhance the signal strength but also affect the peak shape. Pyroelectric performances of devices operating under different bias voltages (0, 0.1, 0.2, and 0.4 V) with a 15.62 mW/cm^2 illumination power density at room temperature are shown in Figure 4a–d. Although the intensity of the signal has been enhanced with bias increasing, there also exist differences of peak shapes at different biases, especially within the threshold. I–t characteristic presented in Figure 4a–d obviously indicates the gradual disappearance of the pyroelectric-effect-induced sharp peak as the bias voltage increase, which is not in line with the changing trend of the overall signal demonstrated above. The reason is that the higher applied bias voltage induced larger dark currents, which in turn increased the background temperatures of the device, resulting in a slighter difference in temperature caused by the low-power-density laser irradiation and thus weakened the pyro-potential in BTO/GaN thin film. Compared with the

https://doi.org/10.1021/acs.nanolett.1c03171
Nano Lett. XXXX, XXX, XXX−XXX

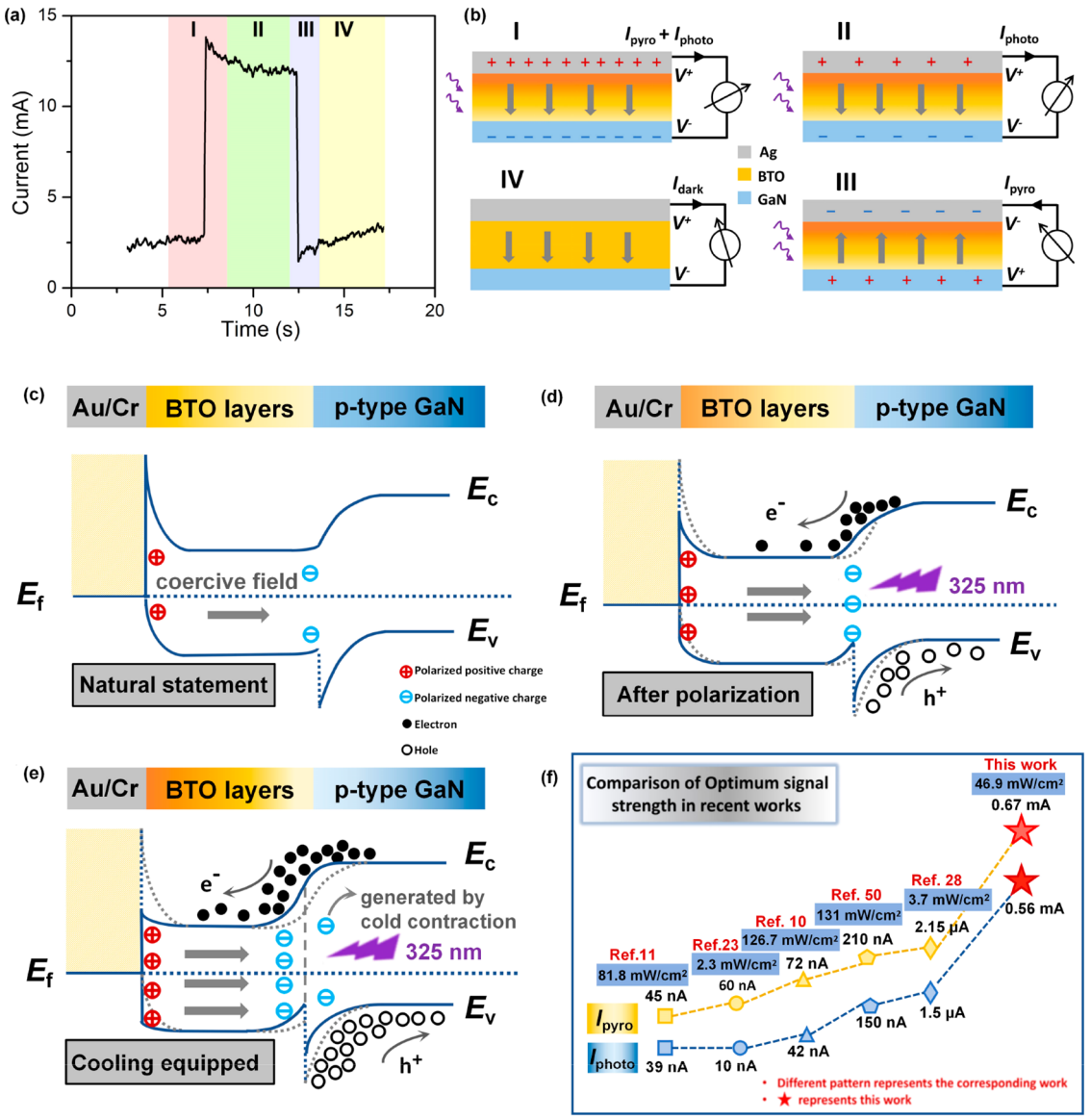

Figure 5. Working mechanism of the self-powered BTO/GaN thin-film PDs. (a) Enlarged plot of a single output period for 325 nm illuminations, divided into four stages, labeled as I, II, III, and IV. (b) Schematic demonstration of the working mechanism in pyro-phototronic processes, corresponding to the four stages labeled in panel a. (c–e) Energy band diagrams for the BTO/GaN thin-film PDs: (c) natural conditions, (d) after DC bias polarization, (e) after being equipped with a cooling system. (f) Comparison chart of recent achievements in related applications.

traditional BTO system response of photoelectric (~100 s),[10,11,21] the BTO/GaN pyro-phototronic response time could be faster (~5 s). The specific response time at different biases with 31.25 mW/cm^2 illumination power density under a cooling system are plotted in Figure 4e. Both response times τ_{pyro} and τ_{photo} are improved from 0.35 to 0.16 s and from about 3.27 to 2.35 s with the bias added, respectively, indicating that the influence of the background temperature caused by the dark current can be ignored because of the much smaller heat accumulation compared with the temperature change caused by laser irradiation at high power density. In a word, the ordinary phototronic effect is the base going through the whole testing process; the pyroelectric effect with higher responsivity and faster response time could be an optimization, whereas the treatments of interface coupling, cooling, and prepolarization provide effective optimizing methods for BTO/GaN thin-film PDs.

2.3. Working Mechanism of the Self-Powered BTO/GaN Thin-Film PDs. The working mechanism for BTO/GaN thin-film PDs could be explained by the pyro-phototronic effect in Figure 5a, b and the energy band diagrams described in Figure 5c–e. The enlarged plot of a a single output period for 325 nm illumination extracted from Figure S2c can be divided into four stages, labeled as I, II, III, and IV as shown in Figure 5a, including a sharp rising edge (I_{pyro} + I_{photo}), a stable plateau (I_{photo}), a falling edge (I_{pyro}), and another stable plateau (I_{dark}) as shown in Figure 5b (see the Supporting Information for a detailed explanation of the pyro-phototronic effect). The structure of the fabricated GaN/BTO thin-film detector can be considered as a BTO layer trapped between Schottky barriers at the left and the heterojunction at the right interfaces as shown in Figure 5c. The formation process of this band structure can be seen in Figure S5. Before polarization, there exists an original coercive filed induced by spontaneous polarization within BTO thin films shown in Figure 5c. A

https://doi.org/10.1021/acs.nanolett.1c03171
Nano Lett. XXXX, XXX, XXX−XXX

ferroelectric polarization is then formed in the BTO thin films after polarization. The positive polarized charges gathered in the left Au/Cr/BTO interface, leading to a decrease in the Schottky barrier. Simultaneously, the negative polarized charges gathered in the right BTO/GaN interface, resulting in an increasing energy barrier of the heterojunction. As presented in Figure 5d, the 325 nm illumination-induced electrons flow along BTO layer to the upper Au/Cr electrode and holes flow along GaN layer until to the lower Au/Cr electrode, and thus the output photocurrent signals could be detected. However, the heat caused by light during the process will weaken the pyro-phototronic effect. To get rid of this, the cooling system was equipped instead of only introducing a single prepolarization treatment. As the temperature decreases, the volume of BTO films will be compressed and a displacement will be generated along its *c*-axis, which will enhance the asymmetry of the material and greatly improve the internal polarization of the material (shown in Figure 5e). There will be more polarized charges at interfaces and plenty of negative polarized charges gathered at the BTO/GaN heterojunction, elevating the energy barrier to provide a stronger driving force for electron flow. However, plenty of positive polarized charges gathered at the Au/Cr/BTO Schottky junction, lowering the Schottky barrier to reduce the obstruction for current flow. Because of the strong driving force and weak obstruction, there will be higher current density flowing through the external circuits, so that stronger photoelectric signals will be detected. Moreover, compared with works in recent years, the signal intensity of this work is relatively the strongest with a short response time as shown in Figure 5f.[10,11,23,28,50]

CONCLUSION

The self-powered BTO/GaN thin-film PDs fabricated by the sol−gel method demonstrate a novel, high-efficiency ultraviolet-sensing system due to the pyro-phototronic coupled effects in comparison with the traditional approaches. The structure of the BTO layer sandwiched between the Schottky barrier formed with the gold electrode and the heterojunction formed with GaN helps to greatly improve the responsivity of the PD with a relatively short response time. With the combination of 325 nm illumination, a cooling system, and prepolarization treatments applied, the fabricated PD system delivers an enhancement of photocurrent and photovoltaic plateaus, which is boosted by up to 1348 and 1052% with faster response times, respectively, as compared with that using the photovoltaic effect alone. Besides, the light-induced self-powered BTO/GaN thin-film PDs can detect the slight signal with a low power intensity efficiently because of the low background temperature derived from the dark current at zero bias. In addition, the application of positive bias to the material can greatly enhance the overall response signal strength, and the application of negative bias to the material can make the intensity of pyroelectric signal more obvious, so the using methods of the PD can be flexibly switched according to different application scenarios to expand its working scope. The BTO/GaN thin-film PDs with pyro-phototronic coupled effects provide a new designing idea for fast and responsive PDs based on a semiconductor and a perovskite, making this environmentally friendly and economical self-powered PD a promising candidate in optoelectronic fields.

ASSOCIATED CONTENT

Supporting Information

The Supporting Information is available free of charge at https://pubs.acs.org/doi/10.1021/acs.nanolett.1c03171.

Experimental process and detailed pyro-phototronic working mechanism of the self-powered BTO/GaN thin-film PDs, structure and characterization of the BTO/GaN thin-film PD (Figure S1), performance of the self-powered BTO/GaN thin-film PDs at different biases (Figure S2), introduction of the cooling system (Figure S3), performance of the self-powered BTO/GaN thin-film PDs under the cooling system (Figure S4), and schematic diagram of band structure formation (Figure S5) (PDF)

AUTHOR INFORMATION

Corresponding Authors

Laipan Zhu − *Center on Nanoenergy Research, School of Physical Science & Technology, Guangxi University, Nanning 530004, China; CAS Center for Excellence in Nanoscience, Beijing Key Laboratory of Micro-nano Energy and Sensor, Beijing Institute of Nanoenergy and Nanosystems, Chinese Academy of Sciences, Beijing 101400, P.R. China; School of Nanoscience and Technology, University of Chinese Academy of Sciences, Beijing 100049, P.R. China;* orcid.org/0000-0001-7538-641X; Email: zhulaipan@binn.cas.cn

Zhong Lin Wang − *Center on Nanoenergy Research, School of Physical Science & Technology, Guangxi University, Nanning 530004, China; CAS Center for Excellence in Nanoscience, Beijing Key Laboratory of Micro-nano Energy and Sensor, Beijing Institute of Nanoenergy and Nanosystems, Chinese Academy of Sciences, Beijing 101400, P.R. China; School of Nanoscience and Technology, University of Chinese Academy of Sciences, Beijing 100049, P.R. China; School of Material Science and Engineering, Georgia Institute of Technology, Atlanta, Georgia 30332, United States;* orcid.org/0000-0002-5530-0380; Email: zhong.wang@mse.gatech.edu

Authors

Yueming Zhang − *Center on Nanoenergy Research, School of Physical Science & Technology, Guangxi University, Nanning 530004, China; CAS Center for Excellence in Nanoscience, Beijing Key Laboratory of Micro-nano Energy and Sensor, Beijing Institute of Nanoenergy and Nanosystems, Chinese Academy of Sciences, Beijing 101400, P.R. China*

Jie Chen − *Center on Nanoenergy Research, School of Physical Science & Technology, Guangxi University, Nanning 530004, China*

Complete contact information is available at: https://pubs.acs.org/10.1021/acs.nanolett.1c03171

Author Contributions

Y.Z., L.Z., and Z.L.W. designed the experiments. Y.Z., J.C., and L.Z. conducted the experiments. All coauthors read and commented on the manuscript.

Notes

The authors declare no competing financial interest.

ACKNOWLEDGMENTS

This research was supported by the National Natural Science Foundation of China (grants 11704032 and 51432005), the National Key R & D Project from Minister of Science and

Technology (2016YFA0202704), and the Beijing Municipal Science & Technology Commission (Z171100000317001, Z171100002017017, and Y3993113DF).

REFERENCES

(1) E, V. R.; Mahajan, A.; Graça, M. P. F.; Mendiratta, S. K.; Monteiro, J. M.; Valente, M. A. Structure and ferroelectric studies of $(Ba_{0.85}Ca_{0.15})(Ti_{0.9}Zr_{0.1})O_3$ piezoelectric ceramics. *Mater. Res. Bull.* **2013**, *48* (10), 4395−4401.

(2) Zhang, Y.; Liang, G.; Tang, S.; Peng, B.; Zhang, Q.; Liu, L.; Sun, W. Phase-transition induced optimization of electrostrain, electrocaloric refrigeration and energy storage of $LiNbO_3$ doped BNT-BT ceramics. *Ceram. Int.* **2020**, *46* (2), 1343−1351.

(3) Novak, N.; Pirc, R.; Kutnjak, Z. Impact of critical point on piezoelectric and electrocaloric response in barium titanate. *Phys. Rev. B: Condens. Matter Mater. Phys.* **2013**, *87* (10), 104102.

(4) Peng, B.; Zhang, Q.; Li, X.; Sun, T.; Fan, H.; Ke, S.; Ye, M.; Wang, Y.; Lu, W.; Niu, H.; Scott, J. F.; Zeng, X.; Huang, H. Giant Electric Energy Density in Epitaxial Lead-Free Thin Films with Coexistence of Ferroelectrics and Antiferroelectrics. *Adv. Electron. Mater.* **2015**, *1* (5), 1500052.

(5) Liang, G.; Zhang, Y.; Zhu, J.; Zhang, Q.; Peng, B. Tailoring and improving the strong-electric-field electrical properties of the BNT-BT ferroelectric ceramics by a functional-group-doping. *Ceram. Int.* **2021**, *47* (5), 6584−6590.

(6) Hao, Y.; Wang, X.; Bi, K.; Zhang, J.; Huang, Y.; Wu, L.; Zhao, P.; Xu, K.; Lei, M.; Li, L. Significantly enhanced energy storage performance promoted by ultimate sized ferroelectric $BaTiO_3$ fillers in nanocomposite films. *Nano Energy* **2017**, *31*, 49−56.

(7) Li, J. J.; Claude, J.; Norena-Franco, L. E.; Seok, S. I.; Wang, Q. Electrical Energy Storage in Ferroelectric Polymer Nanocomposites Containing Surface-Functionalized $BaTiO_3$ Nanoparticles. *Chem. Mater.* **2008**, *20* (20), 6304−6306.

(8) Kim, J.; Kim, Y.; Kim, Y. S.; Lee, J.; Kim, L.; Jung, D. Large nonlinear dielectric properties of artificial $BaTiO_3/SrTiO_3$ superlattices. *Appl. Phys. Lett.* **2002**, *80* (19), 3581−3583.

(9) Zhou, T.; Zha, J. W.; Cui, R. Y.; Fan, B. H.; Yuan, J. K.; Dang, Z. M. Improving dielectric properties of $BaTiO_3$/ferroelectric polymer composites by employing surface hydroxylated $BaTiO_3$ nanoparticles. *ACS Appl. Mater. Interfaces* **2011**, *3* (7), 2184−2188.

(10) Zhao, K.; Ouyang, B.; Bowen, C. R.; Yang, Y. Enhanced photocurrent via ferro-pyro-phototronic effect in ferroelectric $BaTiO_3$ materials for a self-powered flexible photodetector system. *Nano Energy* **2020**, *77*, 105152.

(11) Zhao, K.; Ouyang, B.; Yang, Y. Enhancing Photocurrent of Radially Polarized Ferroelectric $BaTiO_3$ Materials by Ferro-Pyro-Phototronic Effect. *iScience* **2018**, *3*, 208−216.

(12) Mahata, M. K.; Koppe, T.; Mondal, T.; Brusewitz, C.; Kumar, K.; Kumar Rai, V.; Hofsass, H.; Vetter, U. Incorporation of Zn^{2+} ions into $BaTiO_3$: Er^{3+}/Yb^{3+} nanophosphor: an effective way to enhance upconversion, defect luminescence and temperature sensing. *Phys. Chem. Chem. Phys.* **2015**, *17* (32), 20741−20753.

(13) He, Y.; Zhang, T.; Zheng, W.; Wang, R.; Liu, X.; Xia, Y.; Zhao, J. Humidity sensing properties of $BaTiO_3$ nanofiber prepared via electrospinning. *Sens. Actuators, B* **2010**, *146* (1), 98−102.

(14) Lee, M. S.; Meyer, J. U. A new process for fabricating CO_2-sensing layers based on $BaTiO_3$, and additives. *Sens. Actuators, B* **2000**, *68* (1−3), 293−299.

(15) Choi, K. J.; Biegalski, M.; Li, Y. L.; Sharan, A.; Schubert, J.; Uecker, R.; Reiche, P.; Chen, Y. B.; Pan, X. Q.; Gopalan, V.; Chen, L. Q.; Schlom, D. G.; Eom, C. B. Enhancement of ferroelectricity in strained $BaTiO_3$ thin films. *Science* **2004**, *306* (5698), 1005−1009.

(16) Maier, R.; Cohn, J. L. Ferroelectric and ferrimagnetic iron-doped thin-film $BaTiO_3$: Influence of iron on physical properties. *J. Appl. Phys.* **2002**, *92* (9), 5429−5436.

(17) Shin, S. H.; Kim, Y. H.; Lee, M. H.; Jung, J. Y.; Nah, J. Hemispherically Aggregated $BaTiO_3$ Nanoparticle Composite Thin Film for High-Performance Flexible Piezoelectric Nanogenerator. *ACS Nano* **2014**, *8* (3), 2766−2773.

(18) Huan, Y.; Wang, X.; Fang, J.; Li, L. Grain size effect on piezoelectric and ferroelectric properties of $BaTiO_3$ ceramics. *J. Eur. Ceram. Soc.* **2014**, *34* (5), 1445−1448.

(19) Muta, H.; Kurosaki, K.; Yamanaka, S. Thermoelectric properties of doped $BaTiO_3$-$SrTiO_3$ solid solution. *J. Alloys Compd.* **2004**, *368* (1−2), 22−24.

(20) Xiao, X.; Widenmeyer, M.; Xie, W.; Zou, T.; Yoon, S.; Scavini, M.; Checchia, S.; Zhong, Z.; Hansmann, P.; Kilper, S.; Kovalevsky, A.; Weidenkaff, A. Tailoring the structure and thermoelectric properties of $BaTiO_3$ via Eu^{2+} substitution. *Phys. Chem. Chem. Phys.* **2017**, *19* (21), 13469−13480.

(21) Ma, N.; Yang, Y. Enhanced self-powered UV photoresponse of ferroelectric $BaTiO_3$ materials by pyroelectric effect. *Nano Energy* **2017**, *40*, 352−359.

(22) Song, K.; Ma, N.; Mishra, Y. K.; Adelung, R.; Yang, Y. Achieving Light-Induced Ultrahigh Pyroelectric Charge Density Toward Self-Powered UV Light Detection. *Adv. Electron. Mater.* **2019**, *5* (1), 1800413.

(23) Ma, N.; Zhang, K.; Yang, Y. Photovoltaic-Pyroelectric Coupled Effect Induced Electricity for Self-Powered Photodetector System. *Adv. Mater.* **2017**, *29* (46), 1703694.

(24) Wu, L.; Akbashev, A. R.; Podpirka, A. A.; Spanier, J. E.; Davies, P. K. Infrared-to-ultraviolet light-absorbing $BaTiO_3$-based ferroelectric photovoltaic materials. *J. Am. Ceram. Soc.* **2019**, *102* (7), 4188−4199.

(25) Peng, W.; Wang, X.; Yu, R.; Dai, Y.; Zou, H.; Wang, A. C.; He, Y.; Wang, Z. L. Enhanced Performance of a Self-Powered Organic/Inorganic Photodetector by Pyro-Phototronic and Piezo-Phototronic Effects. *Adv. Mater.* **2017**, *29* (23), 1606698.

(26) Wang, Z. L. On Maxwell's displacement current for energy and sensors: the origin of nanogenerators. *Mater. Today* **2017**, *20* (2), 74−82.

(27) Zhang, C.; Tang, W.; Pang, Y.; Han, C.; Wang, Z. L. Active micro-actuators for optical modulation based on a planar sliding triboelectric nanogenerator. *Adv. Mater.* **2015**, *27* (4), 719−26.

(28) Wang, Z.; Yu, R.; Pan, C.; Li, Z.; Yang, J.; Yi, F.; Wang, Z. L. Light-induced pyroelectric effect as an effective approach for ultrafast ultraviolet nanosensing. *Nat. Commun.* **2015**, *6*, 8401.

(29) Kalyani, A. K.; Brajesh, K.; Senyshyn, A.; Ranjan, R. Orthorhombic-tetragonal phase coexistence and enhanced piezoresponse at room temperature in Zr, Sn, and Hf modified $BaTiO_3$. *Appl. Phys. Lett.* **2014**, *104* (25), 252906.

(30) Rabuffetti, F. A.; Brutchey, R. L. Structural evolution of $BaTiO_3$ nanocrystals synthesized at room temperature. *J. Am. Chem. Soc.* **2012**, *134* (22), 9475−87.

(31) Zhang, F.; Li, M.; Zhu, Y.; Zhao, M.; Xie, S.; Wei, M.; Li, Y.; Hu, Z.; Li, M. Ferroelectric polarization enhancement of photovoltaic effects in $BaTiO_3/BiFeO_3/TiO_2$ heterostructure by introducing double-functional layers. *J. Alloys Compd.* **2017**, *695*, 3178−3182.

(32) Song, K.; Zhao, R.; Wang, Z. L.; Yang, Y. Conjuncted Pyro-Piezoelectric Effect for Self-Powered Simultaneous Temperature and Pressure Sensing. *Adv. Mater.* **2019**, *31* (36), 1902831.

(33) Wang, B.; Zhu, Y.; Dong, J.; Jiang, J.; Wang, Q.; Li, S.; Wang, X. Self-powered, superior high gain silicon-based near-infrared photosensing for low-power light communication. *Nano Energy* **2020**, *70*, 104544.

(34) Zhang, Y.; Hu, M.; Wang, Z. Enhanced performances of p-Si/n-ZnO self-powered photodetector by interface state modification and pyro-phototronic effect. *Nano Energy* **2020**, *71*, 104630.

(35) Zhu, L.; Wang, L.; Xue, F.; Chen, L.; Fu, J.; Feng, X.; Li, T.; Wang, Z. L. Piezo-Phototronic Effect Enhanced Flexible Solar Cells Based on n-ZnO/p-SnS Core-Shell Nanowire Array. *Adv. Sci.* **2017**, *4* (1), 1600185.

(36) Zhu, L.; Wang, L.; Pan, C.; Chen, L.; Xue, F.; Chen, B.; Yang, L.; Su, L.; Wang, Z. L. Enhancing the Efficiency of Silicon-Based Solar Cells by the Piezo-Phototronic Effect. *ACS Nano* **2017**, *11* (2), 1894−1900.

https://doi.org/10.1021/acs.nanolett.1c03171
Nano Lett. XXXX, XXX, XXX−XXX

(37) Yin, B.; Zhang, H.; Qiu, Y.; Luo, Y.; Zhao, Y.; Hu, L. The light-induced pyro-phototronic effect improving a ZnO/NiO/Si heterojunction photodetector for selectively detecting ultraviolet or visible illumination. *Nanoscale* **2017**, *9* (44), 17199−17206.
(38) Chaib, H.; Toumanari, A.; Khatib, D.; Kinase, W. Theoretical study of temperature dependence of spontaneous polarization, optical properties and free and clamped linear electrooptic coefficients of $BaTiO_3$ in the tetragonal phase. *Ferroelectrics* **1999**, *234* (1−4), 61−80.
(39) Chaib, H.; Khalal, A.; Nafidi, A. Theoretical Investigation of Spontaneous Polarization and Dielectric Constant of $BaTiO_3/SrTiO_3$ Superlattices. *Ferroelectrics* **2009**, *386*, 41−49.
(40) Zhao, X.; Liu, W.; Chen, W.; Li, S. Preparation and properties of $BaTiO_3$ ceramics from the fine ceramic powder. *Ceram. Int.* **2015**, *41*, S111−S116.
(41) Ma, C.-T.; Gu, Z.-H. Review of GaN HEMT Applications in Power Converters over 500 W. *Electronics* **2019**, *8* (12), 1401.
(42) Muth, J. F.; Lee, J. H.; Shmagin, I. K.; Kolbas, R. M.; Casey, H. C.; Keller, B. P.; Mishra, U. K.; DenBaars, S. P. Absorption coefficient, energy gap, exciton binding energy, and recombination lifetime of GaN obtained from transmission measurements. *Appl. Phys. Lett.* **1997**, *71* (18), 2572−2574.
(43) Lee, H. N.; Christen, H. M.; Chisholm, M. F.; Rouleau, C. M.; Lowndes, D. H. Strong polarization enhancement in asymmetric three-component ferroelectric superlattices. *Nature* **2005**, *433* (7024), 395−399.
(44) Dai, Y.; Wang, X.; Peng, W.; Xu, C.; Wu, C.; Dong, K.; Liu, R.; Wang, Z. L. Self-Powered Si/CdS Flexible Photodetector with Broadband Response from 325 to 1550 nm Based on Pyro-phototronic Effect: An Approach for Photosensing below Bandgap Energy. *Adv. Mater.* **2018**, *30* (9), 1705893.
(45) Li, G.; Li, X.; Zhao, J.; Zhu, Q.; Chen, Y. Strong interfacial coupling effects of ferroelectric polarization with two-dimensional electron gas in $BaTiO_3$/MgO/AlGaN/GaN/Si heterostructures. *J. Mater. Chem. C* **2019**, *7* (19), 5677−5685.
(46) Monemar, B. Fundamental energy gap of GaN from photoluminescence excitation spectra. *Phys. Rev. B* **1974**, *10* (2), 676−681.
(47) Saha, S.; Sinha, T. P.; Mookerjee, A. Electronic structure, chemical bonding, and optical properties of paraelectric $BaTiO_3$. *Phys. Rev. B: Condens. Matter Mater. Phys.* **2000**, *62* (13), 8828−8834.
(48) Bhat, T. N.; Pandey, B. K.; Krupanidhi, S. B. Polarization-induced interfacial coupling modulations in $BaTiO_3$/GaN heterojunction devices. *J. Phys. D: Appl. Phys.* **2017**, *50* (27), 275101.
(49) Bie, Y. Q.; Liao, Z. M.; Zhang, H. Z.; Li, G. R.; Ye, Y.; Zhou, Y. B.; Xu, J.; Qin, Z. X.; Dai, L.; Yu, D. P. Self-powered, ultrafast, visible-blind UV detection and optical logical operation based on ZnO/GaN nanoscale p−n junctions. *Adv. Mater.* **2011**, *23* (5), 649−53.
(50) Ma, N.; Yang, Y. Boosted photocurrent via cooling ferroelectric $BaTiO_3$ materials for self-powered 405 nm light detection. *Nano Energy* **2019**, *60*, 95−102.

https://doi.org/10.1021/acs.nanolett.1c03171
Nano Lett. XXXX, XXX, XXX−XXX